Research Article | Vol. 30, No. 7 / 28 Mar 2022 / Optics Express 10317
Optics EXPRESS

Energy deposition and incubation effects of nonlinear absorption of ultrashort laser pulses in dielectrics

ZIYUE GUO,[1] KAILIN HU,[1] TAO CAO,[1] SHAOZHEN LIU,[1] JIKUN YAN,[1] ZHOU LI,[1] QI XU,[1] PAUL B. CORKUM,[2] AND JIAHUI PENG[1,*]

[1]School of Optical and Electronic Information, Huazhong University of Science and Technology, 1037 Luoyu Road, Wuhan 430074, China
[2]Joint Attosecond Science Laboratory, National Research Council and University of Ottawa, 100 Sussex Drive, Ottawa, ON, K1A 0R6, Canada
*jpeng@hust.edu.cn

Abstract: Although ultrashort laser has been widely employed in micromachining thanks to its excellent processing precision, one of the main challenges it faces when applied to 3D modification inside dielectrics is its processing efficiency. Many applications require multiple pulses to achieve significant modification to create structure such as microlenses. We report incubation experiments on energy deposition and the control of material modification in fused silica. This allows us to develop a practical incubation model by taking account different ionization mechanisms, in which coefficients relating to multiphoton and avalanche ionization change with laser shots due to accumulating defects. We then extend our study to the scheme where a pre-pulse is used to limit the absorption volume through pre-seeding. Both experiments and simulations show that the efficiency of laser processing can be significantly improved without sacrificing the spatial resolution with this method, especially for longer pulses.

1. Introduction

Recently, ultrashort lasers have gained momentum in material processing technologies in response to the increasing demand of laser processing market, which is expected to be over several billions of U.S. dollars and to grow continuously at a moderate rate. Because their pulse durations are shorter than the time scale of thermal diffusions, ultrashort lasers are employed to improve the quality of micromachining and are used for high quality microfabrication of soft materials and biological tissues. Ultrashort lasers are now extensively applied to micromachining transparent materials, including fiber Bragg grating [1], 3D nonlinear photonic crystal in nonlinear optical materials [2,3], holographic patterns inside glass [4], 3D capability of the two-photon polymerization [5], waveguides in optical crystals and ceramics [5–9], microfluidic structures and optofluidic microsystems/devices [10–16], micro-optical components [17–22], nanosurgery of cells and tissues [23], and etc.

When such ultrashort lasers are applied in material processing, it is imperative to employ multiple laser shots. There are mainly two reasons: firstly, from a laser perspective, the single pulse energies of most commercial femtosecond lasers are less than 1 mJ; secondly, from a material processing perspective, laser pulse energies need to be kept at a modest level to achieve reasonable spatial resolution. Of course, it is not hard to obtain lasers with pulse energies larger than 1 mJ, but it is always at the cost of the repetition rate, which means to decrease the efficiency of machining eventually. So, most lasers employed in industrial applications are working at high repetition rate with pulse energies less than 1 mJ. For ultrashort laser processing in transparent materials, the higher the laser pulse energy, the larger the modification volume of the material will be, as we will show in Fig. 1. Solely increasing the pulse energy to improve the modification

#453063 https://doi.org/10.1364/OE.453063
Journal © 2022 Received 5 Jan 2022; revised 27 Feb 2022; accepted 6 Mar 2022; published 14 Mar 2022

Optics EXPRESS

power (or the efficiency of laser micromachining, characterized by the absorbed energy by the material) will deteriorate the resolution (or the quality of laser micromachining) [24].

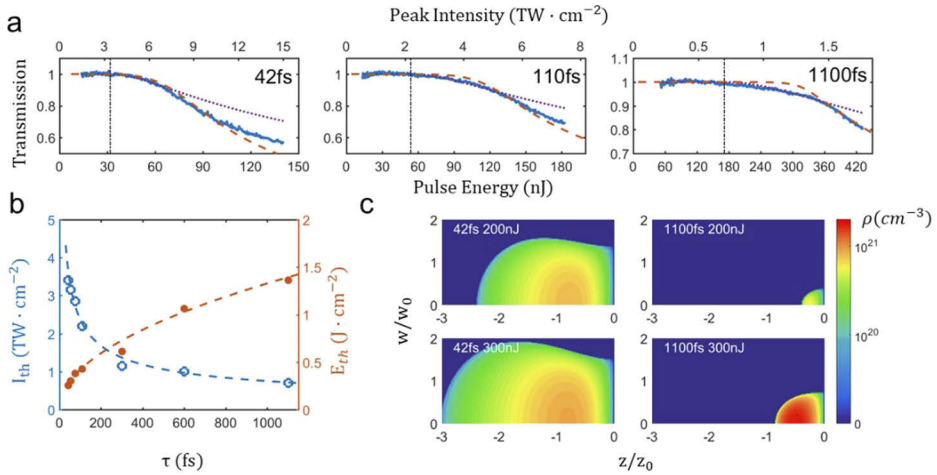

Fig. 1. (a), Nonlinear absorption of three pulse durations: 42 fs, 110 fs, 1100 fs. The blue lines are experimental results showing the transmission as a function of input pulse energy. The purple dotted lines are fittings from "lawn mower" model that mainly takes multiphoton ionization into account, and the red dash lines show the fittings from Eq. (1) that includes both multiphoton and avalanche ionization, the black dot dash line show the threshold E_{th}. (b), The calculated intensity threshold I_{th} and energy threshold E_{th} of nonlinear absorption obtained from (a) at different pulse durations. (c), Modeled spatial distributions of carrier density at 200 nJ and 300 nJ for 42 fs and 1100 fs laser pulses. Here, z is the distance, z_0 is the Rayleigh range, ω is the radius, and the radius of the beam waist w_0 is assumed to be 2μm, which is consistent with our measurements.

A major challenge of ultrashort laser micromachining is, therefore, its efficiency (or numbers of laser shots), which limits the applications to high end products due to the cost and prevents some further extensions due to the lack of mass production capabilities. Therefore, it is practically important to understand how the laser pulses interact with material and its dependence on pulse durations. Meanwhile, how materials react to irradiations laser shot by laser shot should also be clarified, so that, without sacrificing the micromachining quality, the processing efficiency can be maximized (or the least laser shots or energies are employed).

2. Non-linear absorption in dielectrics

Before addressing incubation effects, it is necessary that we demonstrate our understanding of how a single pulse is absorbed when focused inside a dielectric. Under the radiation of ultrashort laser pulse with ultrahigh peak intensities (~10^{13} W/cm^2 in our work), nonlinear ionizations dominate its interaction with dielectrics and the laser energy is deposited inside the material through nonlinear absorption [25]. Nonlinear absorption is achieved via free carrier generation, which are first generated via multiphoton ionization, and then these free carriers seed avalanche ionization to generate more free carriers (absorbing more laser energies). The combination of multiphoton ionization and avalanche ionization can be expressed as

$$dn/dt = W(I) + \alpha In - \frac{n}{\tau}, \tag{1}$$

where n is the density of free carriers, $W(I)$ is the multiphoton ionization rate from the valance band to the conduction band, which is proportional to $\sigma_K I^K$, where σ_K is the K-photon absorption

Optics EXPRESS

cross section, and K is equal to the smallest number of photons needed to overcome the energy bandgap of the material, which is about 9 eV for the sample (fused silica) used in our experiments. Thus, for the 800 nm wavelength (photon energy ~1.6 eV), the K is set to be 6, while $\sigma_6 \approx 4 \times 10^{-13}$ $(\mathrm{TWcm^{-2}})^{-6}\mathrm{cm^{-3}ps^{-1}}$ is obtained by fitting experimental results. I is the time dependent laser intensity, α is the avalanche ionization coefficient, which is 4 $\mathrm{J^{-1}cm^2}$, and τ is the decay (self-trapping) or recombination time of electrons [24], which is set to be 150 fs in the simulation. The total carriers generated by a laser pulse can be expressed as

$$n \approx \left[\int W(I) e^{-\int(\alpha I - \frac{1}{\tau})dt'} dt\right] e^{\int(\alpha I - \frac{1}{\tau})dt} + n_0 e^{\int(\alpha I - \frac{1}{\tau})dt}, \tag{2}$$

where n_0 is the number of initial carriers provided by seeding laser pulses. Under unseeded conditions, the number of initial free carriers is simply $n_0 = 0$.

Here the plasma screening effect is omitted under our experimental conditions. Because the maximum density of free carriers obtained from our simulations (5×10^{20} $\mathrm{cm^{-3}}$) is much smaller than the density of free carriers for the plasma frequency at 800 nm (~1.74×10^{21} $\mathrm{cm^{-3}}$), so the integrated reflection in volume caused by the plasma can be safely omitted.

Thus, the numbers of total free carriers can be calculated by integrating the free carriers' density over time domain and space domain based on the Eq. (2). Since 6 photons are needed to generate each free carrier, the total energy absorbed by the sample as well as the transmission can be calculated. In the simulation, we take into account the propagation of a Gaussian beam along with the ionization process. Because the tightly focused laser beam is used in our experiment (the radius of the beam waist w_0 after being focused by a 0.25 NA microscope objective is about 2μm, and the corresponding peak intensity is clamped at 10^{13} $\mathrm{W/cm^2}$ due to self-limiting nature of the nonlinear adsorption process), so the filamentation and dispersion of pulses play little effect and nonlinear ionizations (i.e. multiphoton ionization and avalanche ionization) predominate here for all the pulse durations used in this work. We also compare the spectrum of the transmitted pulses with the spectrum of the input laser pulse since self-focusing and self-phase modulation are related phenomena, and find that there is little spectral broadening, which confirms that filamentation is not notable under our experimental conditions.

Meanwhile, since multiphoton ionization is a high-order nonlinear process, it is possible to simply describe the process with a threshold behavior – "lawn mower" model, where a threshold of laser intensity, I_{th}, is assumed to be the barrier for nonlinear absorptions and any laser energy with intensity higher than this threshold will be transferred into free carriers. The lawn mower model can describe the propagation of laser beam in dielectrics well, in which the nonlinear absorption mechanism clamps the maximum intensity in the material always close to I_{th}, thus the maximum energy density point is located before the focus [25]. Here I_{th} is not the damage threshold, but an assumption from the "lawn mower" model. Only when the absorbed energy reaches a critical value, will the breakdown in the materials takes place. In lawn mower model, the laser pulse is assumed to maintain a Gaussian-beam shape after interacting with the sample, thus the simulation by this model may deviate in some degree with the practical process when the pulse energy is too high. However, the threshold behavior of the ultrafast laser pulse interaction with dielectrics can be well predicted. And also, in lawn mower model, it is believed that the energy extracted from the beam can counter self-focusing by energy depletion (self-limiting effect) and plasma formation, which means the beam is not undergoing catastrophic self-focusing even when filamentation threshold is nominally exceeded [25].

The measured nonlinear absorption curves (solid lines) at different pulse energies and pulse durations with the simulations obtained from the lawn mower model (dotted lines) and Eq. (1) (dashed lines) are shown in Fig. 1(a). The nonlinear absorption is characterized by the transmission of 800 nm laser pulses at 50 Hz after it being focused to a depth of 70 μm inside a 150 μm thick fused silica sample (Suprasil I, Boston Piezo Optics, Inc, the size is 25 mm×25 mm) with a 0.25 NA microscope objective (evaluated beam waist after focused is 2 μm). The corresponding

Optics EXPRESS

values of the intensity threshold, I_{th}, and energy threshold, E_{th}, are also shown in Fig. 1(b). It is found that I_{th} decreases as the pulse duration increases at the rate of the square root of the pulse duration:

$$I_{th} \propto \frac{1}{\sqrt{\tau}} \left(E_{th} \propto \sqrt{\tau} \right), \tag{3}$$

Meanwhile, the maximum deposited energy density achievable is clamped at I_{th}/c (c is light speed) in the material. Once the energy density exceeds the threshold E_{th}, it will be absorbed by the bulk material, as predicted by the "lawn mower" model. The maximum intensity of the laser pulse (I_{th}) can be reached in the material decreases with $\sqrt{\tau}$, while the energy fluence (E_{th}) increases with $\sqrt{\tau}$. Thus, the longer the pulse duration, the larger the energy can be deposited in the material. Here the dependence of I_{th} and E_{th} on the pulse duration looks very similar to the previous work [26], but I_{th} and E_{th} in our work represent the threshold of nonlinear absorption (any laser energy with intensity higher than this threshold will be transferred into free carriers), not the damage (breakdown) threshold (visible material modification) discussed in [26]. In our experiments, the longest pulse employed is still shorter than 2 ps. So, this $\sqrt{\tau}$ dependence might lose its accuracy once the pulse duration is too long (for example, more than 6.4 ps for fused silica [27]), because the thermal effect and heat diffusion will begin to dominate and lawn mower model alone may not be sufficient to describe the processes.

Even though the "lawn mower" model deviates in some degree at higher energies since it is a typical threshold behavior, it can still shed a light on the density of free carrier generations and its spatial distributions, shown in Fig. 1(c), especially at laser intensities around I_{th}. Clearly, the higher the laser pulse energy the larger the modification volume of the matter will be. Thus, for ultrashort laser micromachining, to achieve high spatial resolution or high quality of the material processing, the laser pulse energies should be kept below a certain level. Meanwhile, we can also compare the estimated free carrier densities at different pulse durations and pulse energies. At lower energy (200 nJ), just 12% above the I_{th} for the 1100 fs pulse, both the modification volume and the maximum free carrier density are smaller for the 1100 fs pulse than those for the 42 fs pulse. However, once the energy is high enough (300nJ, about 50% above the threshold for the 1100 fs pulse), the density of the generated free carriers is significantly larger, though the modification volume is still smaller, for the long pulse (1100 fs). To be specific, while the laser energy increases from 200 nJ to 300 nJ, the modification volumes increase about 50% and 100% and the maxima of free carrier density increase by 13% and 300%, for 42 fs and 1100 fs pulses, respectively.

3. Incubation effects with single-pulse trains

It has been reported that microlens will be formed in materials after being irradiated by hundreds of femtosecond laser pulses [28]. In this process, a bi-convex lens is formed in the pre-focal region. The defocusing of the lens ($\Delta n \approx -1\%$) will cause an increase of the transmission by reducing the peak intensity of the laser pulses. The formation of microlens marks the occurrence of a laser permanent induced modification. In Fig. 2, we show the transmissions of ultrashort laser pulses as a function of laser shots, at pulse durations of 42 fs, 600 fs, 1100 fs, all the experimental parameters are same as those used in Fig. 1. For the 42 fs pulses, it is consistent with the previous report that we do not observe any microlens within 400 laser shots, even at a much higher energy (higher laser intensity too). However, the transmission does drop as the laser shots increase, known as incubation effects (or memory effects) [29]. On the other hand, the transmissions of 600 fs and 1100 fs laser pulses first decrease with the laser shots, as expected from incubation effects, but then increases with further laser shots. We attribute this to the development of a microlens in the material, the specific morphology (geometrical aspects) of the defocusing lens can be found in Ref. [28]. Notably, the pulse energy here is much less than that of the 42 fs pulse. It takes the 600 fs pulse with pulse energy of 243 nJ ($1.8E_{th}$) about 150 shots

Optics EXPRESS

to fabricate a microlens, and it takes the 1100 fs pulse with pulse energy 281 nJ ($1.6E_{th}$) about 70 shots to cause that effect.

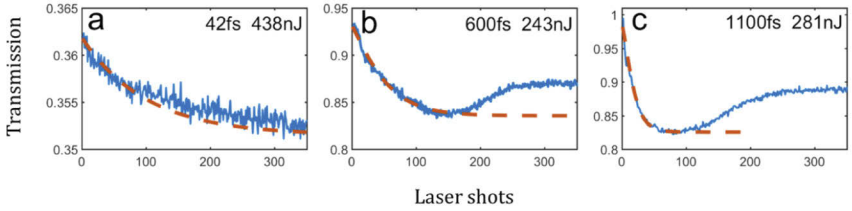

Fig. 2. Nonlinear absorption as a function of laser shots for three pulse durations: 42 fs, 600 fs and 1100 fs. Incubation effect is obvious for all pulse durations and even microlens are generated for longer pulses. Red dash lines are fittings from the "lawn mower" model, in which the incubation coefficient, k, are 0.01, 0.05 and 0.09 for 42 fs, 600 fs and 1100 fs, respectively.

We simulate the incubation effects for three different pulse durations based on the "lawn mower" model and Eq. 4. In which we define the threshold intensity for the nonlinear absorption of a fresh material as $I_{th}(1)$. This threshold will decrease with increasing of laser shots (due to accumulating defects, usually called as memory effect), but eventually saturates at a value, $I_{th}(\infty)$, a sign of permanent damage of the material. Then, the laser intensity threshold for the nonlinear absorption for the Nth laser shot can be expressed as

$$I_{th}(N) = I_{th}(\infty) + [I_{th}(1) - I_{th}(\infty)]e^{-k(N-1)}, \tag{4}$$

where k is the parameter characterizing the incubation power. The larger the value of k, the stronger the incubation effect will be and the less laser shots will be needed to achieve the transmission saturation. The simulation above fits well with experimental results before microlens constructed, shown in Fig. 2 with red dashed lines. Evidently, for the same normalized pulse energy fluence E/E_{th}, it takes longer pulses much fewer laser shots to saturate at the minimum transmission.

To sum up, "lawn mower" model not only can describe the nonlinear absorption of ultrashort laser in dielectrics reasonably well, for pulse durations up to 1.1 ps, but also shows the free carrier density will increase with the pulse duration (as long as the laser intensity is above I_{th}). This explains why sometimes longer pulses cause faster modification of materials, even when their intensities are well below that of shorter pulses. It is also not surprising to see that longer pulses show stronger incubation capabilities, given the free carrier densities are higher for them. Besides, knowing that I_{th} decreases linearly with $1/\sqrt{\tau}$ through the lawn mower model, one can easily estimate I_{th} for different pulse durations and find optimized laser parameters for micromachining.

However, the ultrashort laser micromachining is more than just a threshold behavior. With increasing of pulse duration, the contribution from avalanche ionization plays a more and more important role while contributions from direct multiphoton ionization decreases accordingly. So, there will be an optimized pulse duration, while the balanced contributions from multiphoton ionization and avalanche ionization will give a best laser micromachining efficiency. If we take the microlens as a bench mark, it will take both more laser energy and laser shots to make the microlens for 1100 fs laser pulses compared with 600 fs laser pulses, shown in Fig. 3. Given that 40 fs pulse cannot construct observable microlens within 1000 laser pulses, thus the pulse duration of 600 fs is close to the optimized pulse duration, where the peak laser intensity is high enough to generate a decent number of seeding carriers and the pulse duration is long enough to maximize the avalanche ionization. On the other hand, experiments do show that longer pulse will generate higher density of free carriers, which results in a stronger incubation power. Then

Optics EXPRESS

the smaller laser machining capability of 1100 fs compared with 600 fs comes from its lower intensity.

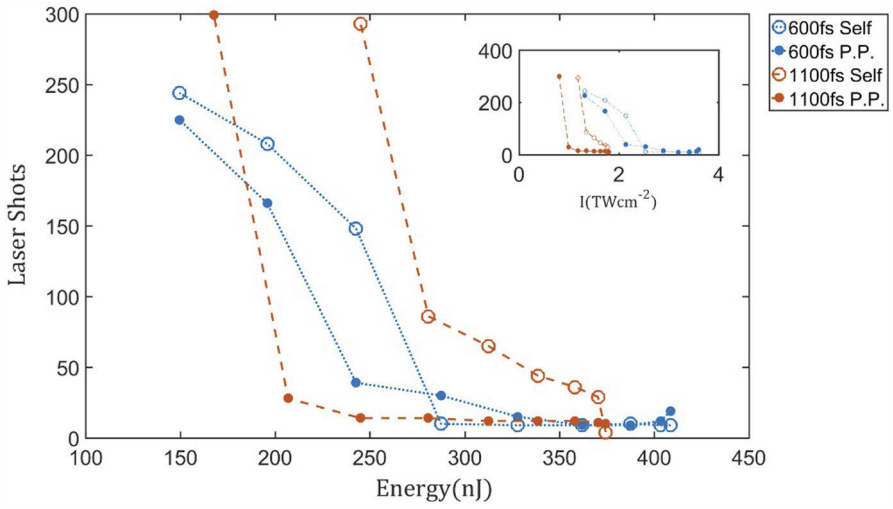

Fig. 3. The number of laser shots used to construct microlens in fused silica for different energies with 600 fs and 1100 fs pulses. The circles show the numbers of the driving laser pulse along, and the points show those with seeding pules, the dash line is to guide the vision.

Shown in Fig. 1(c), the short (fs) laser pulses and long laser pulses show quite different material modification capabilities. The short pulses present good spatial modification capability but with low free carrier densities. On the contrary, long pulses are able to deliver more energy to the target places but with small modification volumes. Thus, in real applications people may find that picosecond lasers are more efficient in cutting thin glasses than femtosecond lasers. However, picosecond lasers have some difficulties in cutting thick glasses because free carriers are confined in the smaller regions along the propagation direction, so that multi-step processing are needed.

4. Double-pulse trains

As Fig. 1(c) demonstrates, there is a conflict between achieving high energy densities and achieving high spatial resolution. We have previously demonstrated that this contradiction can be overcome by using a sequence of two consecutive laser pulses [24]. By employing both short and long pulses in individual steps: a femtosecond pulse (seeding pulse) can be employed in advance to generate initial free carriers to define the modification volumes of the material, and then another longer pulse (driving pulse) can be employed to deposit the laser energies into the material through seeded avalanche ionization. As long as the intensity of the long pulse is kept below I_{th} outside the modification volumes, the modification volumes are solely determined by the seeding (femtosecond) pulse. With the help of seeding laser pulse, the initial free carriers can help to deposit more laser energy into materials [30], leading to improved efficiency while controlling laser modification in the spatial domain, as explained in Fig. 4(c) and 4(d). This control can be done in two manners. If one wants to improve the spatial resolution, which is eventually limited by the diffraction limits of the laser, seeding laser with a shorter wavelength can be employed [31]. If one wants to extend the modification volume, seeding laser with a shorter pulse duration (higher intensity) will be helpful. As one can see from Fig. 1(c), the modification capacity of longer pulses is obtained at the cost of the modification volume. In both cases, seeded avalanche ionization helps to control the spatial resolution and the energy deposition separately.

Optics EXPRESS

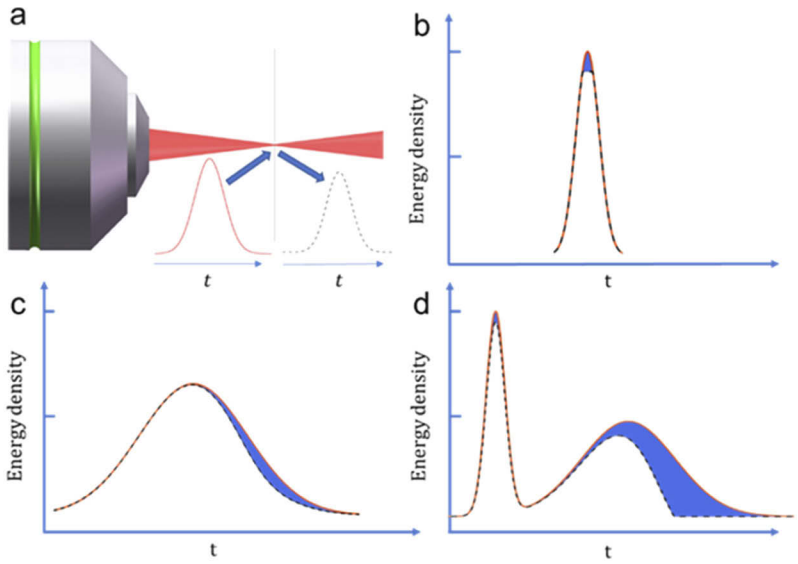

Fig. 4. The energy density (intensity) in time domain before (orange solid line) and after (black dashed line) interacting with the material. Supposing the material is thin enough so that only the ionization process is considered. The blue filling between the two lines shows absorbed energy density by the material in (b) (step function threshold described in "lawn mower" model), (c) (single pulse ionization) and d (seeded avalanche ionization). The free carrier generation equation is used to calculate energy absorption in (c) and (d). The driven pulse in (d) has the same duration as the pulse in (c) and the intensity is lower than that in (c) for the comparison of the absorption ability. The scale in (b), (c) and (d) are the same.

The experiment setup is shown in Fig. 5, where the ultrashort laser is separated into two beams: seeding and driving laser pulse, respectively. A dispersion glass is employed to stretch the driving laser pulse from 42 fs to 1100 fs, so that one can separate the process of initial free carriers' generation and energy deposition. In this way, people can make use of the strength of both femtosecond and picosecond laser pulses simultaneously. The transmission is measured on a shot-to-shot basis, and all data points are averaged over 100 measurements by a Boxcar Integrated Averager (Stanford Research Systems, SR250) to achieve good signal-to-noise ratio. The pulse duration is measured by an autocorrelator with Gaussian pulse shapes assumed and varied by inserting various length of dispersion glass into the laser beam. The delay between seeding pulses and driving pulses is 1 picosecond, which could be tuned from -0.4 ns to 0.4 ns continually by a DC motor linear translation stage (Newport, M-ILS150CC). The overlap of two pulses in time and space is confirmed by the interference pattern in both CCD and spectrometer.

The nonlinear transmission, for driving pulse durations of 42 fs, 600 fs and 1100 fs with similar pulse energies are shown as a function of the number of shots is shown in Fig. 6, with and without the presence of a 70 nJ 42 fs seeding pulse preceding the driving pulse by 1 ps. The time delay of 1 ps is chosen to ensure all the initial free carriers can decay to self-trapped excitons (STEs) [24] for all the pulse durations used in this work, and it is also the practically optimized value in our experiments and the experiences in previous double-pulse work [24]. Notably, the laser intensity of 42 fs pulse is more than 20 times higher than that of the 1100 fs laser pulse. For comparison, the nonlinear transmissions without seeding are also shown with blue lines. Pre-seeding clearly results in greater absorption and, because the volume is contained, higher energy densities.

We propose a practical incubation model to the study of incubation effects under the seeded situation. It has been found that under multi-pulse radiation, the incubation of laser pulses

Optics EXPRESS

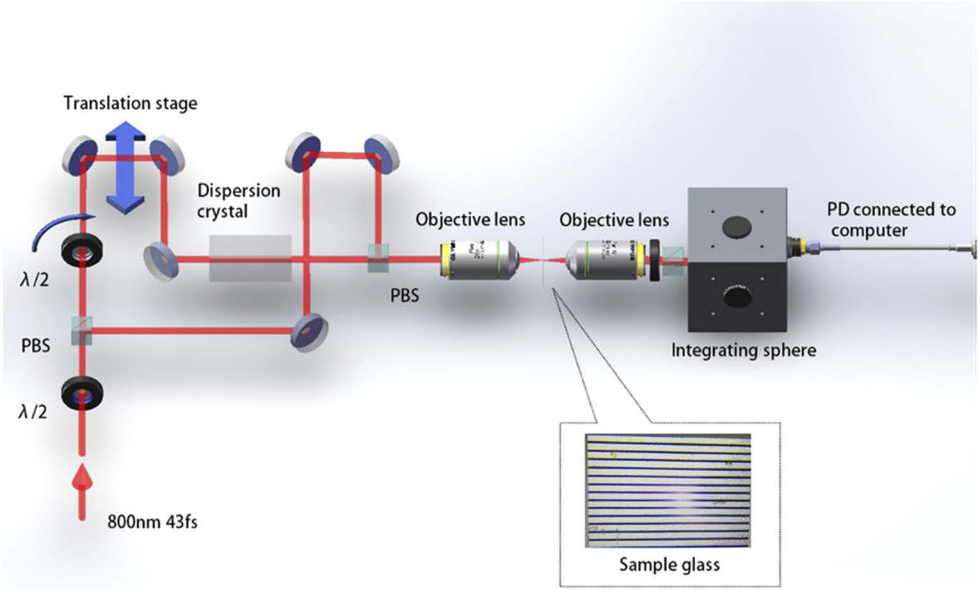

Fig. 5. Experiment setup: laser pulses are from a 800 nm regenerative amplifier Ti:sapphire femtosecond laser operated at 50 Hz; $\lambda/2$ is a half wave-plate; PBS is a polarized beam splitter; Translation stage is used to adjust the delay between the seeding and driving pulses; Dispersion crystal is used to stretch the laser pulse; The sample used here is fused silica.

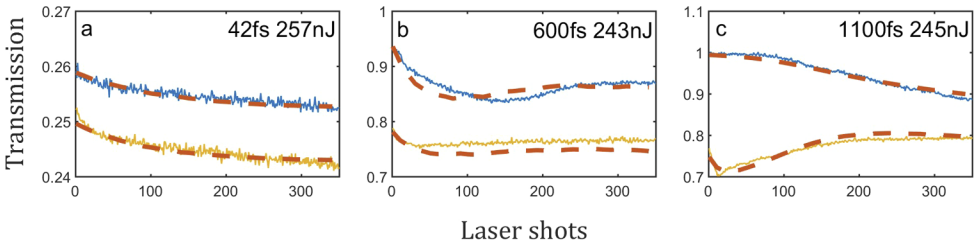

Fig. 6. Using Eq. 1 and our practical incubation model (Eq. 5–7) to simulate the transmission with respect to laser shots to characterize incubation effects quantitatively: experimental values (solid lines) and simulations based on our practical model (dashed lines). The pulse durations are 42 fs (a), 600 fs (b) and 1100 fs (c), the yellow and blue lines correspond to results with and without seeding pulse (energy of seeding pulse is 70 nJ), respectively. The repetition rate is 50 Hz and the pulse separation (time delay) was 1 ps.

Optics EXPRESS

accumulates defects during the processing, making the multiphoton ionization coefficient and avalanche coefficient change shot by shot, this change in ionization cross section indicates a permanent decreasing of its band gap [29]. Thus, the multiphoton absorption cross section coefficient σ_6 and the avalanche ionization coefficient α will increase accordingly, and result in generating more free carries and absorbing more energy from laser pulses. Similarly, we define the dependence of σ_6 and α on laser shots as

$$\sigma_6 = \sigma_6(\infty) + [\sigma_6(1) - \sigma_6(\infty)]e^{-p(N-1)}, \tag{5}$$

$$\alpha(N) = \alpha(\infty) + [\alpha(1) - \alpha(\infty)]e^{-q(N-1)}, \tag{6}$$

where p and q are the factors characterizing the modification rate of σ_6 and α. For the 42 fs pulse, either setting p as 0.08 per shot and q as 0 or setting p as 0 and q as 0.08 per shot can we fit the memory effect. For the 600 fs pulses, only when p is equal to 0.08 per shot and q is equal to 0.04 per shot, can we fit the data well. And for the 1100 fs pulse, only when q is set to be 0.04 per shot can we fit the data well, whereas the changing of multiphoton ionization modification rate p can hardly influence the transmission curves.

It is clear that this model fits well with experimental results at each laser shot and pulse duration. With the seeded free carriers, longer pulses show a better material modification capability than that of short pulses. Clearly, with the presence of free carriers seeding, it can help to deposit more laser energies into the glass, especially for longer pulses. Notably, for the pulse duration of 1100 fs, the pulse energy (245 nJ) is just a little bit over its E_{th} (190 nJ), so the laser energy can barely cause incubation effect alone. However, with the presence of the free carriers seeding, memory effects and even microlens are observable at this energy, a huge distinction compared with shorter pulses. Again, if we make the microlens as the bench mark, it takes much less total laser energies and laser shots to construct microlens for 1100 fs pules when presented seeding free carriers, shown in Fig. 3. This is because avalanche ionization requires no threshold and it is more efficient in generating free carriers, where the carriers increase nearly exponentially as shown in Eq. (2). Therefore, in the seeded avalanche method, picosecond pulses show much higher modification power and machining efficiency than femtosecond pulses.

Even though, the long pulses show stronger material modification power and better material process efficiency when seeded with free carriers, there is still limitation where this better efficiency may not be applicable. Because the free carriers generated via different processes show different behaviors. The free carriers generated via multiphoton process will behave in a more unified and controlled manner, thus show high dependence on the polarizations of the driving laser. However, the inverse bremsstrahlung collisions during the avalanche ionization will wash out this kind of unification, resulting isotropic distributions of the free carriers.

Here we show an example of the difference in processing behavior between femtosecond and picosecond laser pulses by generating microlens. A slide of glass is irradiated by 10^6 shots of laser pulses with duration of 42 fs and energy of 374 nJ, but only 10^3 laser shots for pulse of 1100 fs at 374 nJ to make comparable microlens in the glass. Both pulses are linearly p-polarized. The measured divergences of another laser beam before irradiation and after irradiation are shown in Fig. 7(a) and Fig. 7(b).

Firstly, it confirms again that the power of modification is stronger for longer pulses. With the same laser energy, the machining efficiency is about 1000 times higher for the 1100 fs pulse, even the laser intensity is 26 times higher for 42 fs pulses. Secondly, it shows very different machining results. For the 42 fs lasers, the microlens only affects the divergence of the laser beam along the direction of the polarization. On the other hand, for the 1100 fs lasers the microlens affect the divergence of the laser beam almost evenly in both directions. Because the free carriers generated via multiphoton process will behave in a more unified and controlled manner, but the free carriers generated in avalanche ionization will wash out this kind of unification, resulting isotropic distributions.

Optics EXPRESS

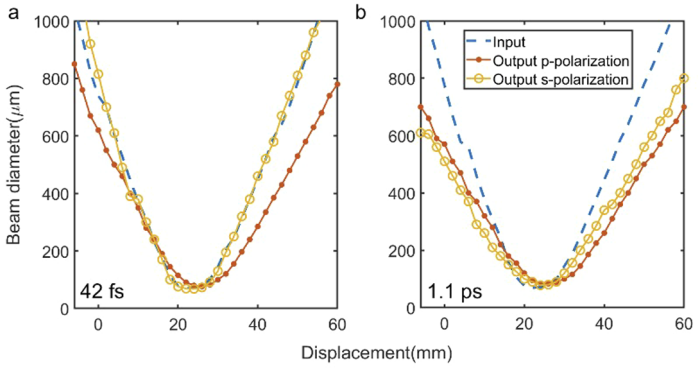

Fig. 7. Laser beam divergences measurements for a fresh material (blue dash lines), and radiated materials, (a) for 10^6 laser shots of a 42 fs 374 nJ p-polarized pulses and (b) for 10^3 laser shots of a 1100 fs 374 nJ p-polarized pulses. Red Solid dots and yellow hollow circles represent the measurements of the same polarization direction as the incident pulse, and the perpendicular direction respectively.

5. Conclusion and discussion

We have shown the nonlinear absorptions of fused silica when it interacts with ultrashort laser pulses, shot by shot, at different pulse durations and pulse energies. These nonlinear absorptions can be fitted in reasonable agreements with experiments via both the lawn mower model and the free carrier generation equation (Eq. (1)), which takes into account both multiphoton ionization and avalanche ionization.

The lawn mower model predicts the nonlinear absorption of the material pretty well near the threshold I_{th}, at least up to 1100 fs pulse. It also shows that I_{th} decreases linearly with square root of pulse duration, $\sqrt{\tau}$. Knowing I_{th} at a certain pulse duration τ, people can easily find optimal laser parameters, which is a handy parameter for real life applications. Once the laser energy is much above the threshold I_{th}, the lawn mower model deviates from the experimental results as the avalanche ionization, an effect without threshold, begins to dominate during the processing.

For the cases of high energy and with pre-seeding of free carriers, using the free carrier generation equation (Eq. (1)), we can well fit the transmission of laser pulse interacting with materials. Further, by setting the multiphoton ionization coefficient $W(I)$ and avalanche ionization coefficient α as a function of laser shots due to the accumulating defects and taking account the change of spot size due to the defocusing of the microlens, our practical incubation model can clarify the memory effects and microlens formations well under the seeded situation.

Both simulations and experiments show that longer pulses can deposit more laser energy into materials and the densities of the generated free carriers are larger for longer pulse at the same energy level. Thus, longer pulses show stronger incubation effects, but its modification volume is limited. For single pulse laser micro-machining, pulses of 600 fs show stronger modification power than those of both 40 fs and 1100 fs pulses, because of the balance of the multi-photon ionization and avalanche ionization. To fully make use of the strength of both short (femtosecond) and long (picosecond) laser pulses, we proposed the application of seeded avalanche ionization. In this case, people can control the spatial resolution and energy deposition separately, and also achieve a good balance between multiphoton ionization and avalanche ionization. The modification efficiency can be improved significantly that both the total laser energies and the laser shots are much smaller in this case, especially for longer pulses.

Even the longer driving pulse show much better modification efficiency, there are limitations of the pulse length and pulse energy. If the driving pulse duration is too long (e.g., nanosecond

Optics EXPRESS

laser pulse), the laser modification volume will expand via heat diffusion, even causing material melting. In order to minimize the heat diffusion and control the damage size, pulse duration generally should be kept short (for example, less than 10 ps for fused silica). Meanwhile, the energy of driving pulse should be limited to prevent free carriers generating from itself outside the region of seeding free carriers.

Further, femtosecond and picosecond laser pulses present quite different processing properties resulting from different contributions of ionization process to the free carrier's generation. The free carriers generated by femtosecond lasers show more uniform spatial distributions (polarization dependent) than those generated by picosecond pulses. Thus, for applications where this unification is desired, the seeded avalanche ionization method may not be the best choice. One may have to be limited to femtosecond lasers and tolerate its lower efficiency.

In addition, this seeded avalanche ionization method also provides a possible way to modify the light fields and pulse shapes, so that the distribution of carriers in three dimensions can be tailored. Then, more complicated and customized structures can be obtained in materials with such laser micromachining.

Funding. National Key Research and Development Program of China (2016YFB1102404); Hubei Technological Innovation Special Fund (2016AAA004).

Acknowledgments. The authors thank David M. Rayner for insightful discussions and help on writing this paper.

Disclosures. The authors declare that there are no conflicts of interest related to this article.

Data availability. Data underlying the results presented in this paper are not publicly available at this time but may be obtained from the authors upon reasonable request.

References

1. A. Martinez and I. Bennion, "Direct writing of fibre Bragg gratings by femtosecond laser," Electron. Lett. **40**(19), 1170–1172 (2004).
2. D. Z. Wei, C. W. Wang, and S. N. Zhu, "Experimental demonstration of a three-dimensional lithium niobate nonlinear photonic crystal," Nat. Photonics **12**(10), 596–600 (2018).
3. T. X. Xu, K. Switkowski, and W. Krolikowski, "Three-dimensional nonlinear photonic crystal in ferroelectric barium calcium titanate," Nat. Photonics **12**(10), 591–595 (2018).
4. Y. Li, W. Watanabe, and Y. Y. Jiang, "Holographic fabrication of multiple layers of grating inside soda–lime glass with femtosecond laser pulses," Appl. Phys. Lett. **80**(9), 1508–1510 (2002).
5. H. B. Sun, S. Matsuo, and H. Misawa, "Three-dimensional photonic crystal structures achieved with two-photon-absorption photopolymerization of resin," Appl. Phys. Lett. **74**(6), 786–788 (1999).
6. K. Sugioka and Y. Cheng, "Femtosecond laser processing for optofluidic fabrication," Lab Chip **12**(19), 3576–3589 (2012).
7. R. R. Gattass and E. Mazur, "Femtosecond laser micromachining in transparent materials," Nat. Photonics **2**(4), 219–225 (2008).
8. R. Osellame, H. J. Hoekstra, G. Cerullo, and M. Pollnau, "Femtosecond laser microstructuring: an enabling tool for optofluidic lab-on-chips," Laser Photonics Rev. **5**(3), 442–463 (2011).
9. F. Chen and J. V. de Aldana, "Optical waveguides in crystalline dielectric materials produced by femtosecond-laser micromachining," Laser Photonics Rev. **8**(2), 251–275 (2014).
10. S. Kawata, H. B. Sun, T. Tanaka, and K. Takada, "Finer features for functional microdevices," Nature **412**(6848), 697–698 (2001).
11. Y. Cheng, K. Sugioka, and K. Midorikawa, "Microfluidic laser embedded in glass by three-dimensional femtosecond laser microprocessing," Opt. Lett. **29**(17), 2007–2009 (2004).
12. Y. Hanada, K. Sugioka, H. Kawano, I. S. Ishikawa, A. Miyawaki, and K. Midorikawa, "Nano-aquarium for dynamic observation of living cells fabricated by femtosecond laser direct writing of photostructurable glass," Biomed. Microdevices **10**(3), 403–410 (2008).
13. Y. Hanada, K. Sugioka, I. Shihira-Ishikawa, H. Kawano, A. Miyawaki, and K. Midorikawa, "3D microfluidic chips with integrated functional microelements fabricated by a femtosecond laser for studying the gliding mechanism of cyanobacteria," Lab Chip **11**(12), 2109–2115 (2011).
14. A. Crespi, Y. Gu, B. Ngamsom, H. J. Hoekstra, C. Dongre, M. Pollnau, R. Ramponi, and R. Osellame, "Three-dimensional Mach-Zehnder interferometer in a microfluidic chip for spatially-resolved label-free detection," Lab Chip **10**(9), 1167–1173 (2010).
15. M. Kim, D. J. Hwang, H. Jeon, K. Hiromatsu, and C. P. Grigoropoulos, "Single cell detection using a glass-based optofluidic device fabricated by femtosecond laser pulses," Lab Chip **9**(2), 311–318 (2009).

Optics EXPRESS

16. D. Choudhury, W. T. Ramsay, R. Kiss, and A. K. Kar, "A 3D mammalian cell separator biochip," Lab Chip **12**(5), 948–953 (2012).
17. A. Schaap, T. Rohrlack, and Y. Bellouard, "Lab on a chip technologies for algae detection: a review," J. Biophotonics **5**(8-9), 661–672 (2012).
18. Y. Cheng, K. Sugioka, K. Midorikawa, M. Masuda, and K. Shihoyama, "Three-dimensional micro-optical components embedded in photosensitive glass by a femtosecond laser," Opt. Lett. **28**(13), 1144–1146 (2003).
19. F. He, Y. Cheng, L. Qiao, and J. Wu, "Two-photon fluorescence excitation with a microlens fabricated on the fused silica chip by femtosecond laser micromachining," Appl. Phys. Lett. **96**(4), 041108 (2010).
20. Y. Shimotsuma, P. G. Kazansky, J. Qiu, and K. Hirao, "Self-organized nanogratings in glass irradiated by ultrashort light pulses," Phys. Rev. Lett. **91**(24), 247405 (2003).
21. V. R. Bhardwaj, E. Simova, P. P. Rajeev, D. M. Rayner, and P. B. Corkum, "Optically produced arrays of planar nanostructures inside fused silica," Phys. Rev. Lett. **96**(5), 057404 (2006).
22. Y. Shimotsuma, M. Sakakura, P. G. Kazansky, and K. Hirao, "Ultrafast Manipulation of Self-Assembled Form Birefringence in Glass," Adv. Mater. **22**(36), 4039–4043 (2010).
23. A. Vogel, J. Noack, G. Huttman, and G. Paltauf, "Mechanism of femtosecond laser surgery of cells and tissues," Appl. Phys. B **81**(8), 1015–1047 (2005).
24. J. Peng, D. Grojo, D. M. Rayner, and P. B. Corkum, "Control of energy deposition in femtosecond laser dielectric interactions," Appl. Phys. Lett. **102**(16), 161105 (2013).
25. D. M. Rayner, A. Naumov, and P. B. Corkum, "Ultrashort pulse non-linear optical absorption in transparent media," Opt. Express **13**(9), 3208–3217 (2005).
26. B. Stuart, M. Feit, S. Herman, A. Rubenchik, B. Shore, and M. Perry, "Nanosecond-to-femtosecond laser-induced breakdown in dielectrics," Phys. Rev. B **53**(4), 1749–1761 (1996).
27. E. G. Gamaly and B. Luther-Davies, "Ablation of solids by femtosecond lasers: Ablation of solids by femtosecond lasers: Ablation mechanism and ablation thresholds for metals and dielectrics," Phys. Plasmas **9**(3), 949–957 (2002).
28. D. Grojo, M. Gertsvolf, H. Jean-Ruel, D. M. Rayner, and P. B. Corkum, "Self-controlled formation of microlenses by optical breakdown inside wide-band-gap materials," Appl. Phys. Lett. **93**(24), 243118 (2008).
29. P. P. Rajeev, M. Gertsvolf, E. Simova, C. Hnatovsky, R. S. Taylor, V. R. Bhardwaj, D. M. Rayner, and P. B. Corkum, "Memory in nonlinear ionization of transparent solids," Phys. Rev. Lett. **97**(25), 253001 (2006).
30. D. Grojo, M. Gertsvolf, S. Lei, T. Barillot, D. M. Rayner, and P. B. Corkum, "Exciton-seeded multiphoton ionization in bulk SiO_2," Phys. Rev. B **81**(21), 212301 (2010).
31. X. Yu, Z. Chang, P. B. Corkum, and S. Lei, "Fabricating nanostructures on fused silica using femtosecond infrared pulses combined with sub-nanojoule ultraviolet pulses," Opt. Lett. **39**(19), 5638–5640 (2014).